Geological Survey of Canada

CURRENT RESEARCH
2003-C28

Fluid evolution and pressure regimes in the Campbell-Red Lake gold deposit, Red Lake mine trend, Red Lake, Ontario: fluid-inclusion evidence for a protracted, highly dynamic hydrothermal system

Guoxiang Chi, Benoît Dubé, and Kenneth Williamson

2003

CURRENT RESEARCH

Natural Resources Canada | Ressources naturelles Canada

Canada

©Her Majesty the Queen in Right of Canada 2003
ISSN 1701-4387

Available in Canada from the
Geological Survey of Canada Bookstore website at:
http://www.nrcan.gc.ca/gsc/bookstore (Toll-free: 1-888-252-4301)

A copy of this publication is also available for reference by depository libraries across Canada through access to the Depository Services Program's website at http://dsp-psd.pwgsc.gc.ca

All requests for permission to reproduce this work, in whole or in part, for purposes of commercial use, resale, or redistribution shall be addressed to: Earth Sciences Sector Information Division, Room 402, 601 Booth Street, Ottawa, Ontario K1A 0E8.

Authors' addresses

Guoxiang Chi *(guoxiang.chi@uregina.ca)*
Department of Geology
University of Regina
3737 Wascana Parkway
Regina, Saskatchewan S4S 0A2

Benoît Dubé *(bdube@nrcan.gc.ca)*
Commission géologique du Canada
880, chemin Sainte-Foy
Québec (Quebec) G1S 2L2

Kenneth Williamson *(kwilliam@nrcan.gc.ca)*
INRS Eau, Terre et Environnement
880, chemin Sainte-Foy
Québec (Quebec) G1S 2L2

Publication approved by GSC Quebec

Original manuscript submitted: 2003-09-17
Final version approved for publication: 2003-10-10

Fluid evolution and pressure regimes in the Campbell-Red Lake gold deposit, Red Lake mine trend, Red Lake, Ontario: fluid-inclusion evidence for a protracted, highly dynamic hydrothermal system

Guoxiang Chi, Benoît Dubé, and Kenneth Williamson

Chi, G., Dubé, B., and Williamson, K. 2003: Fluid evolution and pressure regimes in the Campbell-Red Lake gold deposit, Red Lake mine trend, Red Lake, Ontario: fluid-inclusion evidence for a protracted, highly dynamic hydrothermal system; Geological Survey of Canada, Current Research 2003-C28, 16 p.

Abstract: Fluid inclusions were studied in quartz grains assigned to pre–, syn–, and post–main-stage gold mineralization (Q1, Q2, and Q3) in the Campbell-Red Lake gold deposit. Carbonic fluid inclusions, dominated by CO_2 with variable amounts of CH_4 and N_2, are predominant in all stages. Aqueous inclusions are rare in Q1 and Q2, but common in Q3. Using homogenization temperatures of 350°, 390° and 320°C for aqueous inclusions in Q1, Q2, and Q3 respectively, fluid pressures of up to 2706, 2574, and 1000 bars (corresponding to lithostatic loads of 10.2, 9.7 and 3.8 km) have been obtained from the isochores of carbonic fluid inclusions. Large fluctuations in fluid pressure within individual stages are attributed to variation between lithostatic and subhydrostatic regimes in relation to structural evolution. The extreme scarcity of aqueous inclusions in Q1 and Q2 suggests a 'dry' (water-deficient) carbonic-rich hydrothermal system with CH_4 and N_2, whose gold transporting capacity needs further examination.

Résumé : Au gisement aurifère de Campbell-Red Lake, on a étudié les inclusions fluides contenues dans des cristaux de quartz formés avant, pendant et après le stade principal de minéralisation en or (Q1, Q2 et Q3). Des inclusions fluides carboniques, contenant principalement du CO_2 et des quantités variables de CH_4 et de N_2, sont prédominantes dans toutes les phases de quartz. Les inclusions aqueuses sont rares dans les cristaux de quartz des phases Q1 et Q2, mais courantes dans ceux de la phase Q3. En utilisant respectivement des températures d'homogénéisation des inclusions aqueuses de 350, 390 et 320 °C pour les cristaux de quartz des phases Q1, Q2 et Q3, on a déterminé, à l'aide des isochores des inclusions fluides carboniques, des pressions de fluide correspondantes s'élevant jusqu'à 2706, 2574 et 1000 bars (ce qui se traduit par des charges lithostatiques de 10,2, 9,7 et 3,8 km). Les importantes variations de pression des fluides à l'intérieur d'une même phase sont attribuées à la variation entre les régimes lithostatiques et subhydrostatiques, en rapport avec l'évolution structurale. L'extrême rareté d'inclusions aqueuses dans les cristaux de quartz des phases Q1 et Q2 suggère un système hydrothermal « sec » (présentant un déficit hydrique) caractérisé par une richesse en CO_2 et la présence de CH_4 et de N_2. L'estimation de la capacité de transport de l'or de ce système nécessite des études plus poussées.

INTRODUCTION

The Red Lake mine trend (Fig. 1) is an important auriferous, CO_2-rich, hydrothermal corridor in the Red Lake gold district, Ontario, Canada. It contains the world-class Campbell-Red Lake and the Cochenour-Willans deposits. These deposits are known not only for their high gold grades, but also for their complexity, and consequently the controversy on their genesis. Penczak and Mason (1997) and Damer (1997) proposed a premetamorphic, low-sulphidation, epithermal origin for the Campbell-Red Lake deposit, whereas Andrews et al.(1986), Rogers (1992), Zhang et al.(1997), Tarnocai et al.(1998) , O'Dea (unpub. company rept.), and Twomey and McGibbon (2002), among others, opted for a broadly synmetamorphic-syntectonic origin. A pre- to syn- to late-deformation multistage model was proposed by MacGeehan and Hodgson (1982). Dubé et al. (2001, 2002, 2003) emphasized the protracted nature of hydrothermalism and deformation and the syn-D_2 timing of the high-grade silicic replacement of the carbonate vein.

The nature of the hydrothermal system(s) related to gold mineralization, i.e., epithermal versus 'mesothermal' (also known as orogenic), is important for further exploration in the district as these two styles of gold mineralization show significant variations in terms of setting, geometry, and timing relative to deformation and metamorphism, and consequently of exploration models. Since epithermal and 'mesothermal-orogenic' systems differ most significantly in their formation depths, it is believed that fluid inclusions, which can provide information about fluid pressures and compositions, can be used to help discriminate these origins. Fluid inclusions have been studied in the Campbell Mine (Tarnocai, 2000) and the Goldcorp Inc. High Grade zone in the Red Lake mine (Chi et al., 2002). The study by Chi et al. (2002) suggested significant fluctuations in fluid pressures during carbonate veining and gold-associated silicification and sulphidization (arsenopyrite) of the carbonate veins and host rocks. However, uncertainties remained as to whether the large variation in fluid pressures may be related to post-trapping modification of the fluid inclusions. The primary objective of this study is to verify these uncertainties with further fluid-inclusion petrographic and microthermometric work, plus some laser-Raman analyses of the gas composition of fluid inclusions. In addition to the samples examined in the last study (KG00-50, KG00-11) (Chi et al., 2002), which were from the Red Lake mine, we have also included another sample from the Red Lake mine (Core A, courtesy Robert S. Penczak), one from the Cochenour area (BD20-98A), and one sample from the Campbell mine (RP94-20A, courtesy Robert S. Penczak). A sample from a quartz-carbonate vein (KG00-51A) cutting a lamprophyre dyke from the Red Lake mine, which clearly cuts the main zones of high-grade mineralization but is itself locally cut by 'remobilized' gold mineralization (e.g. Dubé et al., 2002; Twomey and McGibbon 2002), was also studied. With the analyses of this set of samples, we aim to better understand the evolution of the hydrothermal system in terms of fluid composition, temperature, and pressure, from pre-, through syn-, to post-mineralization stages.

In our previous study (Chi et al., 2002), we focused on fluid inclusions in ankerite that show growth zones outlined by fluid inclusions. However, ankerite has two shortcomings for fluid inclusion study. One is that it is difficult to differentiate fluid inclusions distributed along growth zones and those superimposing on them, because the crystals are densely populated by fluid inclusions of different generations. The second shortcoming is that fluid inclusions in carbonate crystals are relatively prone to post-trapping modification. Therefore, in this study, we choose to focus on fluid inclusions in quartz because they are relatively more resistant to post-trapping modification. In addition, the relatively clean nature of quartz allows the use of the 'fluid-inclusion assemblage' concept (Goldstein and Reynolds, 1994) to internally constrain the validity of the microthermometric data.

GEOLOGICAL SETTING

The Red Lake mine trend is part of the Red Lake gold district, located in the Red Lake greenstone belt in western Ontario. The Red Lake greenstone belt consists of 2.99–2.89 Ga Mesoarchean rocks dominated by volcanic rocks, and 2.75–2.73 Ga Neoarchean volcanic rocks, separated by an angular unconformity (Sanborn-Barrie et al., 2001). Two main episodes of penetrative deformation (D_1, D_2) took place after the ca. 2.74 Ga volcanism (Sanborn-Barrie et al., 2001), resulting in two sets of folds (F_1 and F_2) and associated foliation (S_1 and S_2).

The Red Lake mine trend contains the Campbell-Red Lake and the Cochenour-Willans deposits (Fig. 1). These deposits are hosted by volcanic rocks of the Mesoarchean Balmer assemblage (2.99 Ga), which was subject to a north-trending, large-scale, F_1 folding superimposed by southeast-trending F_2 folding (Fig. 1). Flattened F_{2a} folds with highly strained limbs, southeast-trending faults and associated CO_2-rich alteration and gold mineralization define a southeast-trending structural lineament known as the Cochenour–Gullrock Lake deformation zone (Andrews et al., 1986) or the Red Lake mine trend (Dubé et al., 2002, 2003). This hydrothermal corridor is traced from the Campbell-Red Lake deposit to at least the Cochenour mine to the northwest and corresponds to a zone of heterogeneous, protracted D_2 strain (Fig. 1). Both the mineralization zones and their host rocks are cut by feldspar porphyries (FP) and lamprophyre dykes (*see* Dubé et al., 2001, 2002, 2003).

Gold mineralization is associated with arsenopyrite-rich silicic replacement of carbonate veins and breccias as well as enclosing wall-rock selvages. Dubé et al. (2001, 2002, 2003) have shown several lines of evidence that extensive carbonate veining, characterized by cavity-fill colloform-crustiform and cockade textures indicative of higher rate of dilation than crystal growth, is mainly a pre- to early-D_2 event, whereas the bulk of the gold mineralization and associated arsenopyrite-rich silicification is mainly syn-D_2. However, mineralization is not a simple process going from carbonate-veining to silicification-gold mineralization, because multiple stages of carbonate veining have been documented, including those in the gold-silicification stage and those cutting lamprophyre dykes

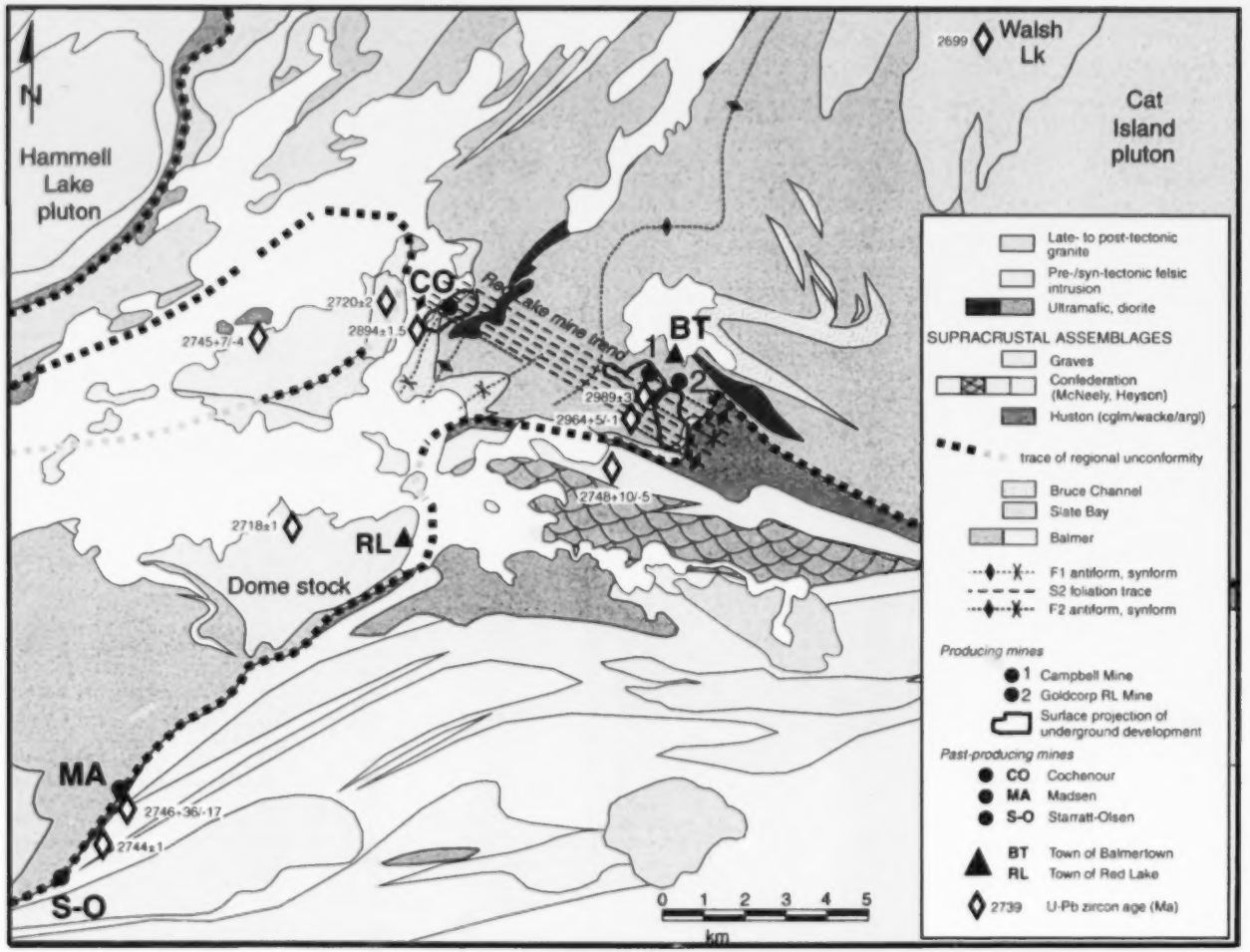

Figure 1. *Geological map of the Red Lake mine Trend area (modified from Sanborn-Barrie et al., 2001, and Goldcorp geological data; after Dubé et al., 2003).*

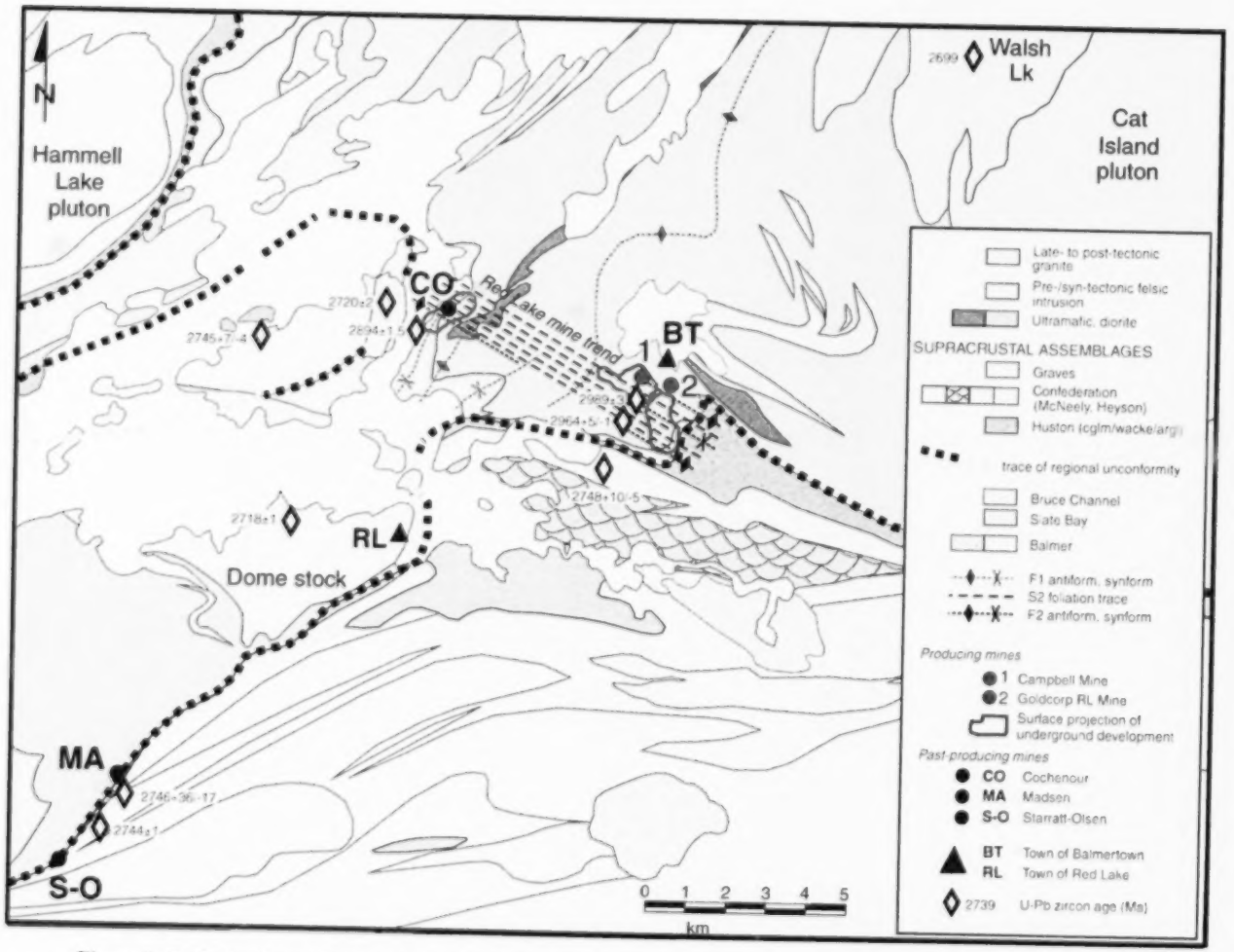

Figure 1. *Geological map of the Red Lake mine Trend area (modified from Sanborn-Barrie et al., 2001, and Goldcorp geological data; after Dubé et al., 2003).*

(Dubé et al., 2003). The quartz-carbonate veins in the lamprophyre dykes are essentially composed of calcite and euhedral quartz crystals perpendicular to the vein walls. These en échelon extensional veins postdate the main stage of gold mineralization. Late gold remobilization is demonstrated by visible gold coating and filling fractures hosted within a steeply dipping lamprophyre dyke (Dubé et al., 2002; Twomey and McGibbon, 2002). Based on these observations, Dubé et al. (2003) concluded that the Red Lake mine trend formed from one or more protracted multistage alteration and veining events with pre- and early-D_2 iron-carbonate and aluminous alteration followed by syn-D_2 silicification and gold precipitation as well as some late carbonatization and gold remobilization postdating lamprophyre dykes.

PETROGRAPHY OF THE SAMPLES FOR FLUID-INCLUSION STUDY

Eight doubly polished thin sections were studied for fluid inclusions. The petrographic features of these samples are summarized in Figure 2.

All the samples contain carbonates and quartz, and some of them contain sulphides and gold. The carbonate veins show colloform-crustiform-cockade textures (Fig. 2A-F). Two kinds of carbonate are differentiated based on potassium ferricyanide–Arizarin Red S staining and cathodoluminescence. The majority of the carbonate is ankerite, which is characterized by dark blue staining (Fig. 2D) and nonluminescence. A second type of carbonate is calcite, which is characterized by red staining (Fig. 2H) and yellow luminescence. Ankerite is the main component of pre–high-grade mineralization carbonate veins, and is commonly deformed to variable degrees ranging from undulation extinction to subgrains. Calcite is found in en échelon extensional veins postdating mineralization, is typically associated with euhedral quartz, and is not deformed.

Three types of quartz are differentiated based on their petrographic features and paragenesis (Q1, Q2, and Q3). Q1 is coarse, euhedral to subhedral, and is in growth contact with ankerite presumably predating gold mineralization (KG00-50 and RP94-20A) (Fig. 3A-C). This type of quartz is interpreted to have precipitated contemporaneously or penecontemporaneously with the ankerite. Coarse quartz crystals cutting ankerite in a sterile vein (BD20-98A) are also assigned to Q1. Q2 is generally fine grained, and is associated with sulphides and gold mineralization (Fig. 3F). In sample Core-A, which is from an interval grading 2.641 oz/t gold over 2 feet, both coarse-and fine-grained quartz crystals (Fig. 3D and E) are assigned to Q2. Q3 is euhedral and is found in a quartz vein cutting the post-ore lamprophyre dyke. Q1 and Q2 show variable degrees of deformation, whereas Q3 is relatively strain-free.

FLUID-INCLUSION PETROGRAPHY AND MICROTHERMOMETRY

Fluid inclusions were studied in the three types of quartz described above. Fluid inclusions occurring in isolation (randomly distributed), clusters, and intracrystal short trails are considered primary or pseudosecondary. Examples of different kinds of occurrences are shown in Figure 4. Individual clusters or short trails of fluid inclusions are considered as fluid inclusion assemblages, within which fluid inclusions are assumed to have been entrapped at the same time.

Most of the fluid inclusions occurring in quartz are CO_2-dominant, as are those in carbonate (Chi et al., 2002). These inclusions do not contain any visible aqueous phase at room temperature, even when the inclusions are very large (e.g. Fig. 4C). Aqueous fluid inclusions are scarce in Q1 and Q2 quartz, but are more abundant in Q3. Consequently, few total homogenization temperature data have been obtained except for Q3.

The microthermometric measurements were carried out on a USGS heating/freezing stage located at University of Regina. The accuracy and precision of the measurements of melting and homogenization temperatures of carbonic phases are about ±0.2°C, whereas those of total homogenization temperatures are around ±1°C. The microthermometric results are listed in Table 1, and shown in Figures 5, 6, and 7. The data of Chi et al. (2002) are included in the figures for comparison.

The melting temperatures of CO_2 (T_m-CO_2) range from -56.5° to -59.2°C for the three generations of quartz as a whole (Fig.5; Table 1), indicating that the fluids are dominated by CO_2, plus variable amounts of other gases. With the exception of one sample (BD20-98A) (Table 1), fluid inclusions from the Q1 stage appear to have slightly higher T_m-CO_2 (mainly -56.6° to -57.3°C) (Fig. 5A) than those from ore-stage quartz (mainly -56.7° to -57.5°C) (Fig. 5B). T_m-CO_2 values from Q3 are lower than Q1 and Q2, mainly ranging from -57.2° to -58.0°C (Fig. 5C).

The homogenization temperatures of CO_2 (T_h-CO_2) are highly variable for the three generations of quartz together, as well as for individual generations of quartz (Fig.6; Table 1). However, fluid inclusions within individual 'fluid-inclusion assemblages' show a relatively narrow range of T_h-CO_2 (*see* Table 1 for clusters or trails of fluid inclusions), suggesting that the variation in T_h-CO_2 between different fluid-inclusion assemblages are not caused by post-trapping modifications.

Only a few aqueous fluid inclusions were found in Q1 quartz, and their homogenization temperatures (T_h) range from 152.7°–172.5°C (Fig. 7A). Note that the large variation in T_h in one fluid-inclusion assemblage (170.8–470.0°C; RP94-20A, Table 1) probably reflects heterogeneous trapping or post-trapping modifications, and the minimum value is adopted. Higher T_h values have been reported for some aqueous inclusions in ankerite in Chi et al. (2002), ranging from 190°–350°C (Fig. 7A). The melting temperatures of ice have been measured in one sample, and range from -22.7° to -21.3°C (BD20-98A, Table 1). The T_h values of a few aqueous inclusions have been measured in Q2 quartz (Chi et al., 2002),

(A) KG00-50-3 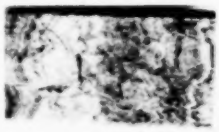	Composed of coarse, elongated to blocky ankerite with well developed growth zones. The crustiform texture seen on the slab is outlined by the growth zones. The ankerite is moderately deformed. A few elongated quartz crystals are associated with the ankerite. This quartz is contemporaneous with ankerite, both predating gold mineralization. A few fluid inclusions are studied in the quartz (**Q1**). (From Red Lake mine)
(B) KG00-50-5	Coarse, blocky ankerite with locally well developed growth zones. Slightly to moderately deformed. Some euhedral quartz is associated with calcite, neither of which are deformed. The ankerite is pre-mineralization, whereas the calcite and euhedral quartz are post-mineralization. These two minerals are the two principal subjects of study in Chi et al. (2002). A second type of quartz, which is associated with ankerite and deformed, is the subject of the present study (**Q1**). Fine-grained, strongly deformed ankerite. (From Red Lake mine)
(C) RP94-20A	Carbonatized host rock. Fine to coarse ankerite, strongly deformed. Quartz, strongly deformed. Most quartz crystals are fine grained, but some are coarse and elongated. Coarse quartz crystals are commonly partly replaced by or deformed to fine quartz. Fluid inclusions are studied in the residual coarse quartz (**Q1**) associated with ankerite. (From Campbell mine)
(D) BD20-98A	Blocky to elongated ankerite, strongly deformed and micro-fractured. Vein of quartz cutting ankerite. Coarse elongated crystals perpendicular to vein wall, strongly deformed. Fluid inclusions are studied in quartz (**Q1**). (From Cochenour)
(E) Core-A2 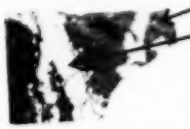	Ankerite, which is strongly deformed, and is characterized by blue staining. Early quartz on the walls of the vein, followed and cut by ankerite (note the fissures in quartz filled by ankerite). Most quartz is fine grained. Some quartz is coarse and elongated; it is commonly partly replaced by or deformed to fine quartz. Fluid inclusions are studied in the residual coarse quartz (**Q2**). From a section running 2.641 oz/t gold. (From Red Lake mine)
(F) Core-A3	From the same core as Core-A2. Ankerite (white) is strongly deformed, and is cut or replaced by quartz (grey). Many of the quartz crystals are coarse and elongated, and are partly replaced by or deformed to fine quartz. Fluid inclusions are studied in the residual coarse quartz (**Q2**). Quartz Ankerite (From Red Lake mine)
(G) KG00-11	Silicified ankerite vein. Gold is associated with siliceous replacement. Quartz is fine grained. Fluid inclusions are studied in quartz (**Q2**). Gold Siliceous replacement Ankerite (From Red Lake mine)
(H) KG00-51A 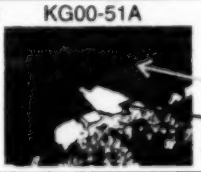	A calcite-quartz vein cutting a lamprophyre dyke. The calcite is characterized by red staining. Quartz is euhedral. Both calcite and quartz are not deformed. Fluid inclusions are studied in quartz(**Q3**). Calcite Quartz (From Red Lake mine)

Figure 2. *Petrographic characteristics of the samples for fluid-inclusion study.*

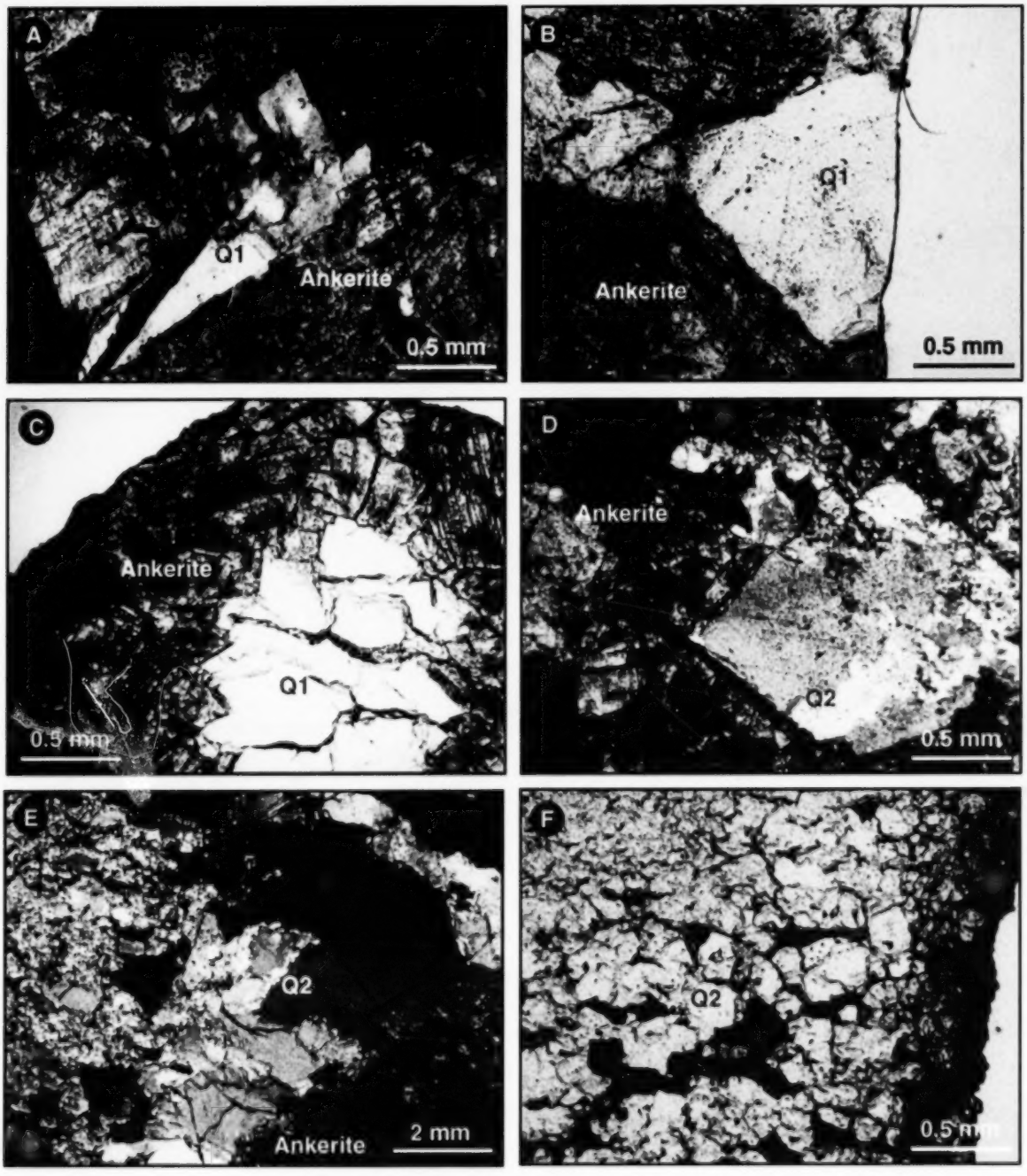

Figure 3. *Petrographic features of different generations of quartz from which fluid inclusions are studied. (**A**) An euhedral quartz crystal (Q1) showing growth contact with coarse, blocky ankerite crystals. Note the undulation interference colour of the quartz related to deformation. Sample KG00-50-3. (**B**) Subhedral quartz crystals (Q1) showing growth contact with coarse, blocky ankerite crystals. Sample KG00-50-5. (**C**) Subhedral quartz crystals (Q1) filling the open space left by ankerite. Sample RP94-20A. (**D**) An euhedral quartz crystal (Q2) partly replaced by ankerite and by finer-grained quartz. Sample Core-A2. (**E**) Elongated quartz crystals (Q2) in a vein cutting ankerite. Note the undulation interference colour and the transformation to or replacement by finer-grained quartz. Sample Core-A3. (**F**) Fine-grained quartz (Q2) associated with gold, replacing ankerite. Sample KG00-11.*

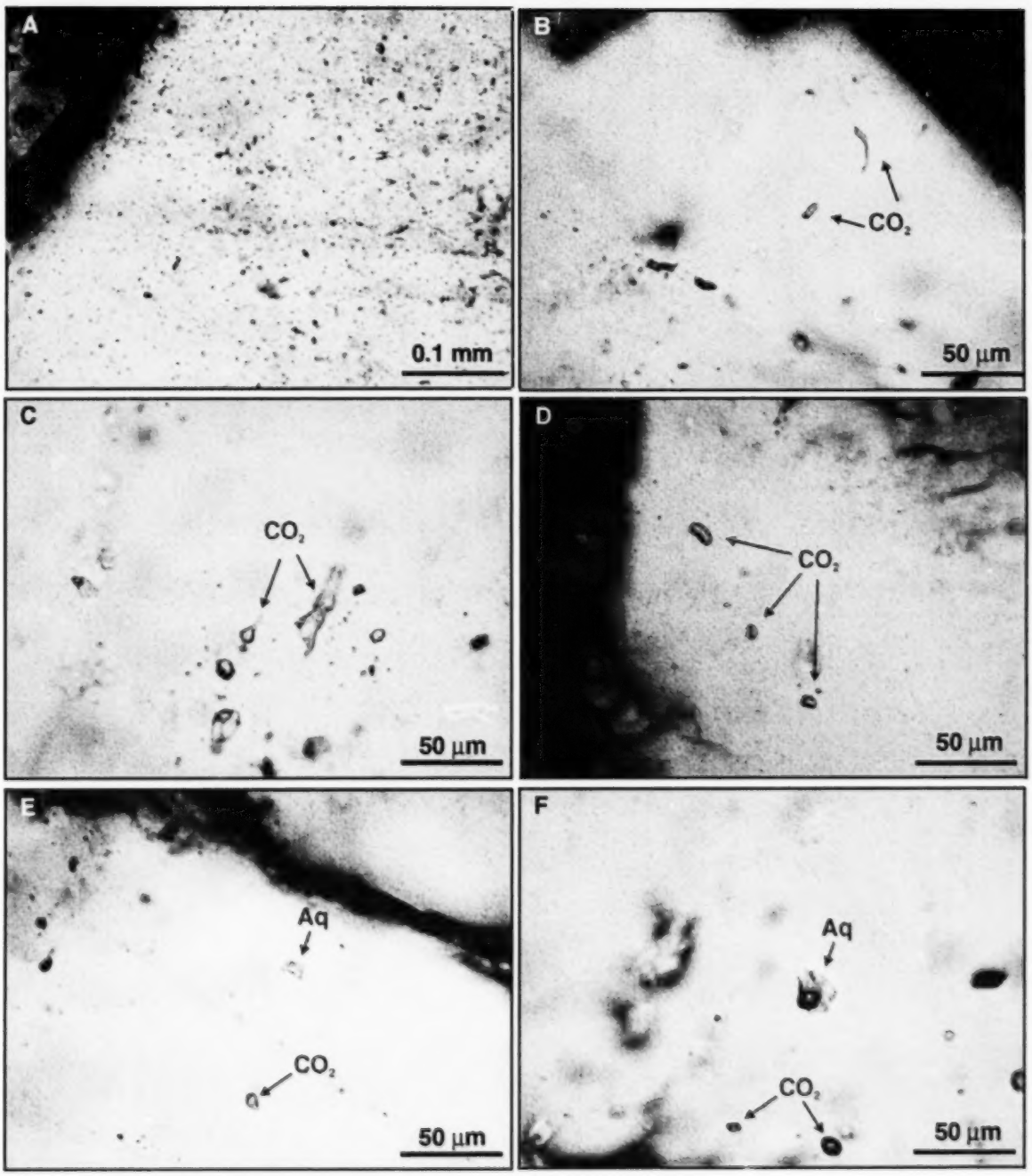

Figure 4. *Different modes of occurrence of fluid inclusions considered as primary or pseudosecondary. (**A**) Randomly distributed fluid inclusions (CO_2) in a Q2 quartz; individual fluid inclusions are relatively isolated and do not show any microfracture or growth zone control. Core-A2. (**B**) Isolated fluid inclusions (CO_2) in a Q1 quartz. KG00-50-3. (**C**) A cluster of fluid inclusions (CO_2) in a Q1 quartz. KG00-50-5. (**D**) A short trail of fluid inclusions (CO_2) in a Q1 quartz. RP94-20A. (**E**) Isolated fluid inclusions (CO_2 and aqueous) in a Q1 quartz. BD20-98A. (**F**) Isolated fluid inclusions (CO_2 and aqueous) in a Q3 quartz. KG00-51A.*

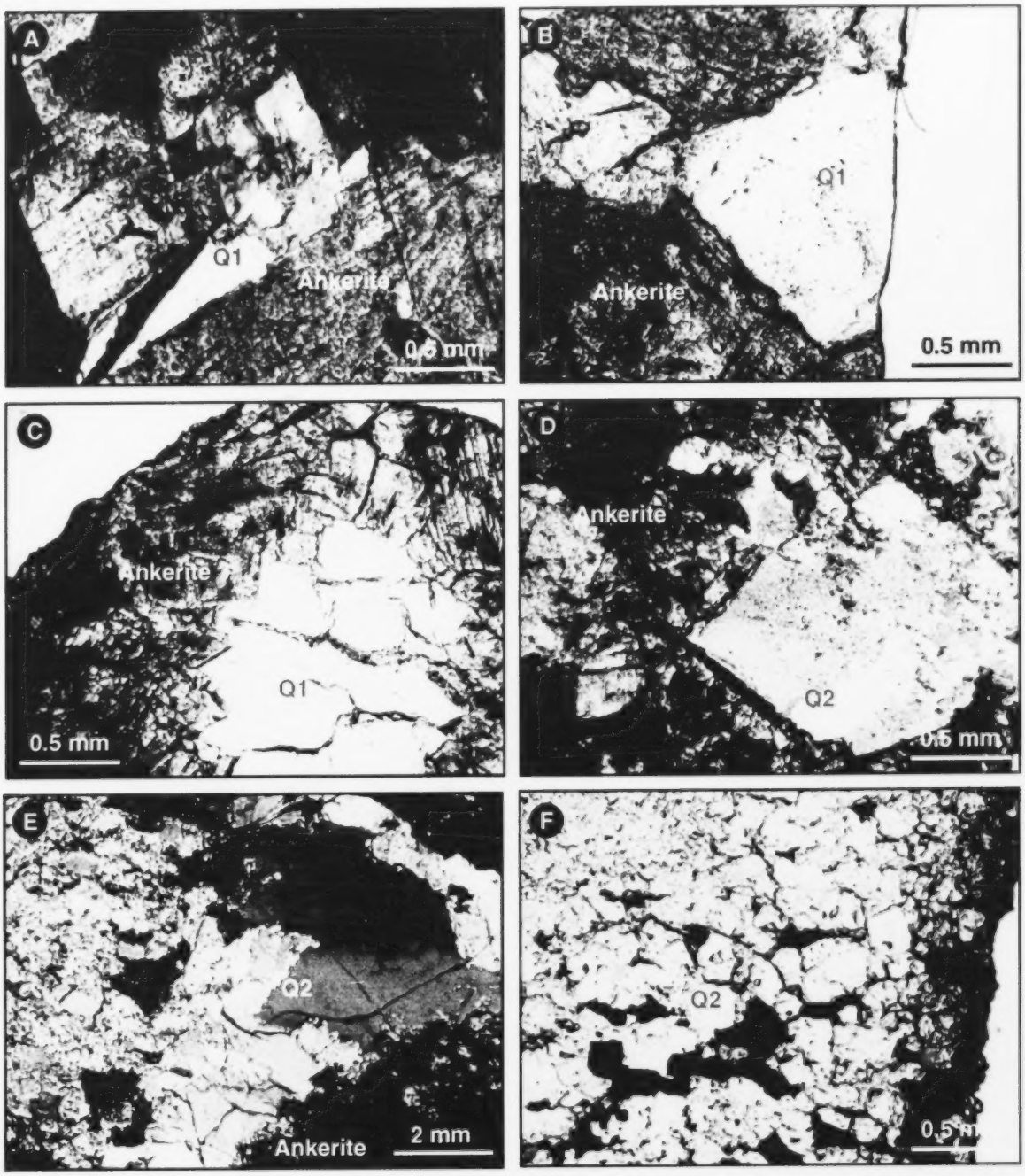

Figure 3. *Petrographic features of different generations of quartz from which fluid inclusions are studied. (**A**) An euhedral quartz crystal (Q1) showing growth contact with coarse, blocky ankerite crystals. Note the undulation interference colour of the quartz related to deformation. Sample KG00-50-3. (**B**) Subhedral quartz crystals (Q1) showing growth contact with coarse, blocky ankerite crystals. Sample KG00-50-5. (**C**) Subhedral quartz crystals (Q1) filling the open space left by ankerite. Sample RP94-20A. (**D**) An euhedral quartz crystal (Q2) partly replaced by ankerite and by finer-grained quartz. Sample Core-A2. (**E**) Elongated quartz crystals (Q2) in a vein cutting ankerite. Note the undulation interference colour and the transformation to or replacement by finer-grained quartz. Sample Core-A3. (**F**) Fine-grained quartz (Q2) associated with gold, replacing ankerite. Sample KG00-11.*

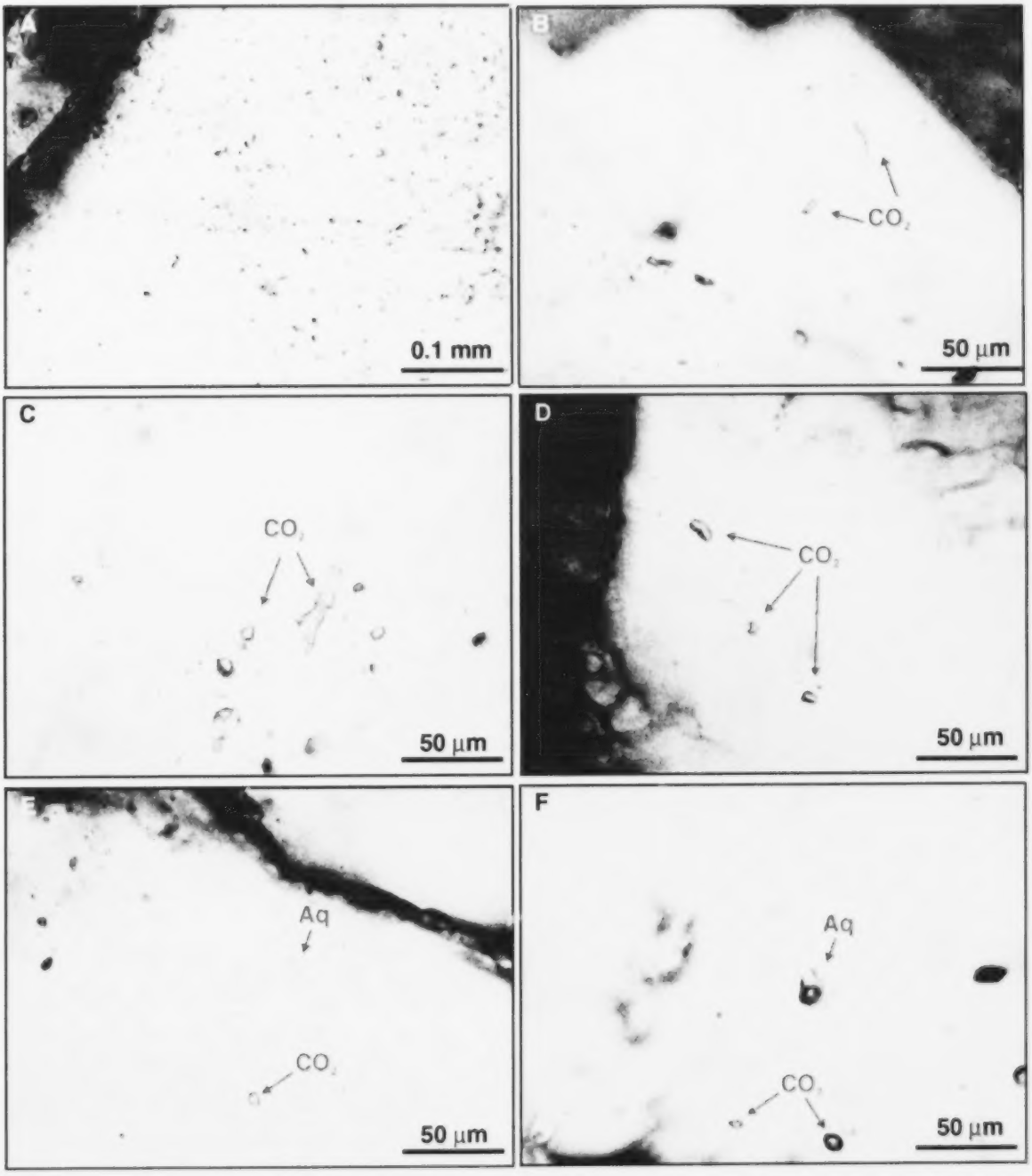

Figure 4. *Different modes of occurrence of fluid inclusions considered as primary or pseudosecondary. (**A**) Randomly distributed fluid inclusions (CO_2) in a Q2 quartz: individual fluid inclusions are relatively isolated and do not show any microfracture or growth zone control. Core-A2. (**B**) Isolated fluid inclusions (CO_2) in a Q1 quartz. KG00-50-3. (**C**) A cluster of fluid inclusions (CO_2) in a Q1 quartz. KG00-50-5. (**D**) A short trail of fluid inclusions (CO_2) in a Q1 quartz. RP94-20A. (**E**) Isolated fluid inclusions (CO_2 and aqueous) in a Q1 quartz. BD20-98A. (**F**) Isolated fluid inclusions (CO_2 and aqueous) in a Q3 quartz. KG00-51A.*

ranging from 250°–390°C (Fig. 7B). No additional measurements have been made in this study. Fluid inclusions in Q3 quartz show T_h values from 135.5°–325.8°C (Fig. 7C). Relatively low T_h values (70°–190°C) for Q3 have been previously reported in Chi et al. (2002) (Fig. 7C). The aqueous fluid inclusions from Q3 commonly show fairly high melting temperatures of clathrate (29.4°–32.6°C, Table 1), indicating the presence of H_2S (Bény et al., 1982). The same observations were made in a previous study (Chi et al., 2002). Some aqueous inclusions in Q3 contain a nahcolite crystal as identified by laser Raman analysis.

Table 1. Fluid inclusion microthermometric data.

Sample	Host mineral	Occurrence	Raman analysis no.	Size (μm)	V/T %	$T_{m\text{-}CO_2}$ (°C) Mean (n)	$T_{m\text{-}H_2O}$ (°C) Mean (n)	$T_{m\text{-}clath}$ (°C) Mean (n)	$T_{h\text{-}CO_2}$ (°C) Range	$T_{h\text{-}CO_2}$ (°C) Mean (n)	T_h (°C) Range	T_h (°C) Mean (n)
KG00-50-3	Q1	Isolated		20	100	-57.0 (1)	-	-	22.7 V	22.7 (1)	-	-
(Red Lake)		Isolated		8	100	-57.0 (1)	-	-	24.5 V	24.5 (1)	-	-
KG00-50-5	Q1	Cluster	b6, b7, b8	20 ~ 55	100	-56.6 (3)	-	-	11.3 ~ 11.3 V	11.3 (3)	-	-
(Red Lake)		Short trail	b11	10 ~ 15	100	-56.6 (3)	-	-	10.8 V	10.8 (1)	-	-
		Isolated	b13	35	100	-56.6 (1)	-	-	13.3 V	13.3 (1)	-	-
		Isolated	b14	23	100	-56.6 (1)	-	-	1.9 V	1.9 (1)	-	-
		Cluster	b18	13 ~ 15	100	-56.6 (2)	-	-	19.3 V	19.3 (1)	-	-
		Isolated	b31	50	100	-56.6 (1)	-	-	14.7 V	14.7 (1)	-	-
		Isolated	b25	18	100	-56.5 (1)	-	-	8.8 V	8.8 (1)	-	-
		Long trail	b24	5 ~ 15	100	-56.9 (2)	-	-	27.8 ~ 28.4 L	28.1 (5)	-	-
RP94-20A	Q1	Short trail	a1, a2, a3	2 ~ 20	100	-56.6 (4)	-	-	3.7 ~ 10.8 L	6.1 (6)	-	-
(Campbell)		Isolated		5	100	-57.0 (1)	-	-	23.3 L	23.3 (1)	-	-
(Barren)		Isolated		5	100	-56.7 (1)	-	-	14.5 L	14.5 (1)	-	-
		Short trail		3 ~ 4	100	-57.1 (1)	-	-	15.5 ~ 16.6 L	16.1 (2)	-	-
		Isolated		6	100	-57.5 (1)	-	-	19.6 L	19.6 (1)	-	-
		Short trail		3 ~ 5	100	-56.9 (1)	-	-	19.6 ~ 19.8 L	19.7 (2)	-	-
		Cluster		3 ~ 4	100	-57.2 (1)	-	-	16.2 ~ 16.5 L	16.4 (2)	-	-
		Isolated		5	100	-57.2 (1)	-	-	-2.4 L	-2.4 (1)	-	-
		Cluster		10	100	-57.1 (1)	-	-	9.7 L	9.7 (1)	-	-
		Isolated		7	100	-57.1 (1)	-	-	15.9 L	15.9 (1)	-	-
		Isolated		9	100	-57.0 (1)	-	-	10.9 L	10.9 (1)	-	-
		Isolated		8	100	-57.0 (1)	-	-	14.5 L	14.5 (1)	-	-
		Cluster		7 ~ 11	15	-	-	-	-	-	170.8 ~ 470.0	170.8 (4)
BD20-98A	Q1	Cluster		3 ~ 11	100	-58.2 (2)	-	-	13.5 ~ 14.4 L	13.8 (5)	-	-
(Cochenour)		Isolated		10	100	-58.4 (1)	-	-	13.8 L	13.8 (1)	-	-
(Barren)		Cluster		6 ~ 11	100	-58.1 (1)	-	-	5.9 ~ 8.3 L	7.2 (4)	-	-
		Isolated		10	100	-58.5 (1)	-	-	5.4 L	5.4 (1)	-	-
		Isolated		10	100	-57.1 (1)	-	-	12.1 L	12.1 (1)	-	-
		Isolated		12	100	-58.2 (1)	-	-	5.2 L	5.2 (1)	-	-
		Isolated		8	100	-58.3 (1)	-	-	-4.1 L	-4.1 (1)	-	-
		Cluster		4 ~ 7	100	-57.4 (2)	-	-	-2.5 ~ 6.5 L	1.3 (3)	-	-
		Isolated		8	100	-57.1 (1)	-	-	6.9 L	6.9 (1)	-	-
		Cluster		6 ~ 7	100	-57.2 (1)	-	-	-3.8 ~ -1.8 L	2.9 (4)	-	-
		Cluster		5 ~ 11	10	-	-22.6 (1)	-	-	-	146.8 ~ 158.2	152.7 (3)
		Isolated		12	10	-	-21.3 (1)	-	-	-	164.3	164.3 (1)
		Cluster		6 ~ 8	10	-	-22.7 (1)	-	-	-	159.4 ~ 185.6	172.5 (2)
Core-A2	Q2	Isolated		6	100	-56.8 (1)	-	-	5.9 L	5.9 (1)	-	-
(Red Lake)		Isolated		6	100	-56.7 (1)	-	-	7.6 L	7.6 (1)	-	-
		Isolated		5	100	-56.8 (1)	-	-	6.3 L	6.3 (1)	-	-
		Isolated		5	100	-56.9 (1)	-	-	8.9 L	8.9 (1)	-	-
		Isolated		8	100	-56.8 (1)	-	-	5.4 L	5.4 (1)	-	-
		Isolated		5	100	-56.8 (1)	-	-	6.3 L	6.3 (1)	-	-
		Isolated		7	100	-56.8 (1)	-	-	8.0 L	8.0 (1)	-	-
		Isolated		6	100	-56.8 (1)	-	-	8.4 L	8.4 (1)	-	-
		Isolated		6	100	-56.8 (1)	-	-	8.6 L	8.6 (1)	-	-
		Isolated		8	100	-56.7 (1)	-	-	6.7 L	6.7 (1)	-	-
		Isolated		7	100	-56.8 (1)	-	-	12.7 L	12.7 (1)	-	-
		Isolated		6	100	-56.7 (1)	-	-	0.3 L	0.3 (1)	-	-
		Cluster		5 ~ 8	100	-56.9 (1)	-	-	10.0 ~ 10.2 L	10.1 (3)	-	-

$T_{m\text{-}CO_2}$ = melting temperature of CO_2; $T_{m\text{-}H_2O}$ = melting temperature of ice; $T_{m\text{-}clath}$ = melting temperature of clathrate;
$T_{h\text{-}CO_2}$ = homogenization temperature of CO_2; T_h = total homogenization temperature; V/T = vapor / total ratio.

GAS COMPOSITION OF CARBONIC FLUID INCLUSIONS

The gas compositions of the carbonic fluid inclusions have been analyzed with laser Raman microspectrometry. The analyses were carried out at le Centre de Recherches sur la Géologie des Matières Premières Minérales et Energétiques (CREGU), UMR, G2R, Nancy, France, with a LABRAM Jobin-Yvon system. The wavelength of the exciting laser is 514 nm, and the carrier gas is ionized Ar. The results of analysis are listed in Table 2, and shown in Figure 8.

Table 1. (cont.)

Sample	Host mineral	Occurrence	Raman analysis no.	Size (μm)	V/T %	$T_{m\text{-}CO_2}$ (°C) Mean (n)	$T_{m\text{-}H_2O}$ (°C) Mean (n)	$T_{m\text{-}clath}$ (°C) Mean (n)	$T_{h\text{-}CO_2}$ (°C) Range	$T_{h\text{-}CO_2}$ (°C) Mean (n)	T_h (°C) Range	T_h (°C) Mean (n)
Core-A3	Q2	Cluster		10 - 12	100	-57.0 (1)	-	-	16.0 - 16.9 V	16.5 (2)	-	-
(Red Lake)		Isolated		25	100	-57.2 (1)	-	-	19.8 V	19.8 (1)	-	-
		Isolated		4	100	-57.4 (1)	-	-	20.6 L	20.6 (1)	-	-
		Isolated		4	100	-57.2 (1)	-	-	21.5 L	21.5 (1)	-	-
		Isolated		13	100	-57.1 (1)	-	-	20.2 L	20.2 (1)	-	-
		Isolated		14	100	-57.1 (1)	-	-	20.5 L	20.5 (1)	-	-
		Isolated		10	100	-57.1 (1)	-	-	25.9 L	25.9 (1)	-	-
KG00-11	Q2	Cluster	a5	5 - 8	100	-56.8 (3)	-	-	20.5 - 21.6 L	20.9 (3)	-	-
		Short trail	a7, a9	5 - 13	100	-56.8 (3)	-	-	13.4 - 14.8 L	14.1 (3)	-	-
		Short trail		9	100	-56.7 (1)	-	-	20.0 L	20.0 (1)	-	-
		Cluster	a3	8	100	-56.8 (1)	-	-	17.0 L	17.0 (1)	-	-
		Cluster	b6, b7	7 - 8	100	-56.7 (2)	-	-	22.6 - 22.7 L	22.7 (2)	-	-
		Isolated	b8	4	100	-56.8 (1)	-	-	10.8 L	10.8 (1)	-	-
		Cluster	c3	4 - 18	100	-56.9 (2)	-	-	20.3 - 22.8 L	21.6 (2)	-	-
KG00-51A	Q3	Cluster		5 - 8	100	-57.2 (1)	-	-	19.7 - 21.7 L	20.4 (3)	-	-
		Cluster		3 - 8	100	-57.8 (1)	-	-	15.0 - 15.8 L	15.3 (3)	-	-
		Cluster		8 - 10	100	-	-	-	22.1 - 22.2 L	22.2 (2)	-	-
		Isolated		12	100	-	-	-	22.1 L	22.1 (1)	-	-
		Cluster		3 - 13	100	-57.4 (1)	-	-	22.2 - 22.5 L	22.4 (3)	-	-
		Cluster		4 - 7	100	-57.8 (1)	-	-	16.6 - 16.7 L	16.7 (2)	-	-
		Short trail		4 - 8	100	-57.4 (1)	-	-	18.1 - 20.4 L	19.6 (3)	-	-
		Cluster	b1, b2	12 -15	100	-57.6 (1)	-	-	26.2 - 26.2 L	26.2 (2)	-	-
		Long trail	b4, b5, b6	7 -15	100	-57.4 (3)	-	-	26.7 - 26.9 L	26.8 (3)	-	-
		Isolated	b9	15	100	-57.7 (1)	-	-	14.3 L	14.3 (1)	-	-
		Isolated	b7	26	100	-57.8 (1)	-	-	17.5 L	17.5 (1)	-	-
		Isolated	b8	15	100	-57.9 (1)	-	-	14.2 L	14.2 (1)	-	-
		Short trail	c2, c3	18 -23	100	-57.6 (3)	-	-	18.6 - 19.6 L	19.0 (3)	-	-
		Isolated	c5	48	100	-57.2 (1)	-	-	28.8 V	28.8 (1)	-	-
		Isolated	c6	30	100	-57.5 (1)	-	-	19.3 L	19.3 (1)	-	-
		Isolated	c7	28	100	-57.5 (1)	-	-	19.5 L	19.5 (1)	-	-
		Isolated	c8	12	100	-57.6 (1)	-	-	21.2 L	21.2 (1)	-	-
		Isolated	c12	10	100	-57.3 (1)	-	-	20.6 L	20.6 (1)	-	-
		Isolated	c14	9	100	-57.5 (1)	-	-	20.9 L	20.9 (1)	-	-
		Isolated	c9	50	100	-56.7 (1)	-	-	0.9 V	0.9 (1)	-	-
		Isolated	c10	38	100	-56.7 (1)	-	-	1.5 V	1.5 (1)	-	-
		Isolated	c15	46	100	-57.6 (1)	-	-	20.1 L	20.1 (1)	-	-
		Cluster		7 -15	100	-	-	-	18.9 - 20.3 L	19.6 (2)	-	-
		Cluster	c20, c21	7 -13	100	-	-	-	19.5 - 20.3 L	20.0 (3)	-	-
		Cluster		15 -30	100	-57.7 (3)	-	-	19.3 - 20.2 L	20.0 (3)	-	-
		Cluster	c24	16 -20	100	-57.2 (1)	-	-	25.6 - 25.7 L	25.7 (2)	-	-
		Isolated	c25	45	100	-57.5 (1)	-	-	17.4 L	17.4 (1)	-	-
		Isolated		16	25	-	-	32.6 (1)	-	-	251.8	251.8 (1)
		Isolated		12	25	-	-	31.6 (1)	-	-	325.8	325.8 (1)
		Isolated		16	25	-	-2.2	31.1 (1)	-	-	254.8	254.8 (1)
		Cluster		11	20	-	-	30.4 (1)	-	-	226.0	226.0 (1)
		Isolated		8	15	-	-	30.6 (1)	-	-	177.0	177.0 (1)
		Isolated		3	15	-	-	-	-	-	198.9	198.9 (1)
		Isolated		9	15	-	-	-	-	-	289.9	289.9 (1)
		Isolated		5	15	-	-	-	-	-	235.9	235.9 (1)
		Isolated		53	10	-	-	-	-	-	193.9	193.9 (1)
		Cluster		12 -15	10	-	-	29.4 (1)	-	-	132.8 - 139.9	135.5 (3)
		Isolated		15	10	-	-	-	-	-	130.8	130.8 (1)

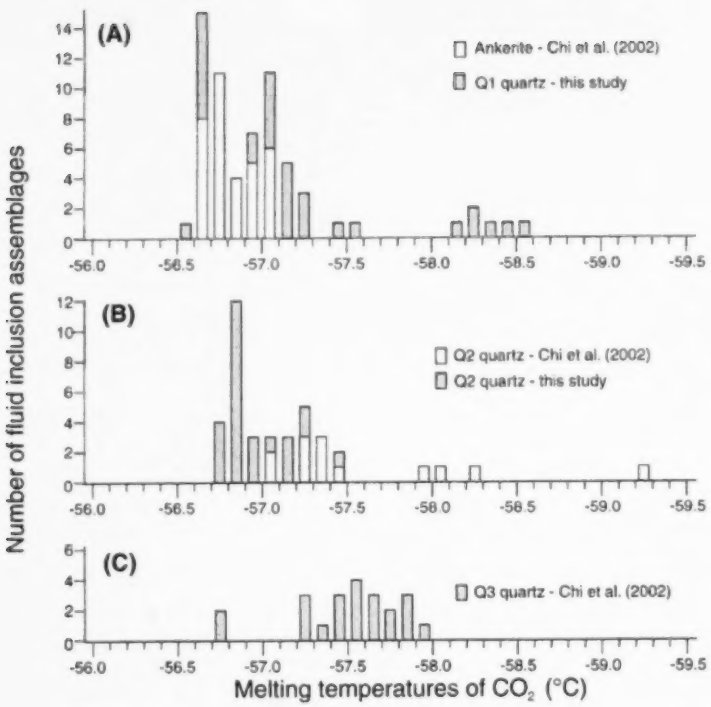
(A)
Ankerite - Chi et al. (2002)
Q1 quartz - this study
(B)
Q2 quartz - Chi et al. (2002)
Q2 quartz - this study
(C)
Q3 quartz - Chi et al. (2002)
Number of fluid inclusion assemblages
Melting temperatures of CO_2 (°C)

Figure 5.

*Histograms of melting temperatures of CO_2 of fluid inclusions from three different generations of quartz. (**A**) Pre-mineralization Q1, (**B**) Ore-stage Q2, and (**C**) Post-mineralization Q3. The data from Chi et al. (2002) are also shown.*

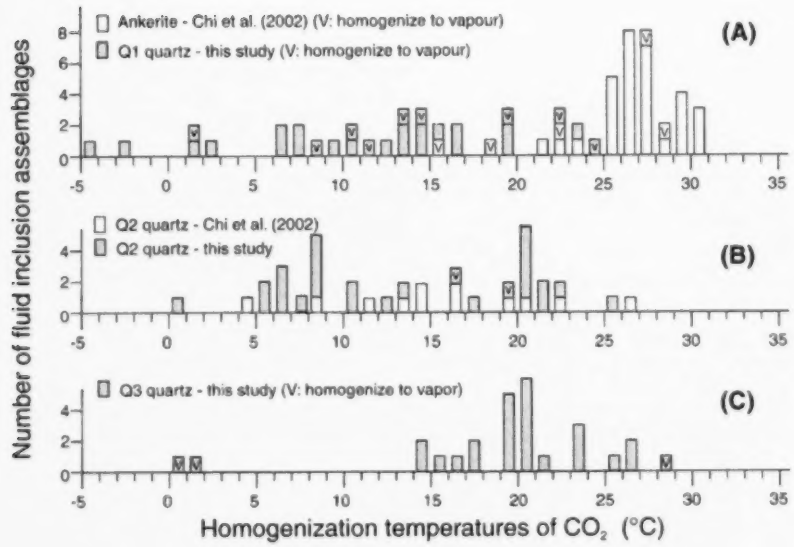
Ankerite - Chi et al. (2002) (V: homogenize to vapour)
Q1 quartz - this study (V: homogenize to vapour)
(A)
Q2 quartz - Chi et al. (2002)
Q2 quartz - this study
(B)
Q3 quartz - this study (V: homogenize to vapor)
(C)
Number of fluid inclusion assemblages
Homogenization temperatures of CO_2 (°C)

Figure 6.

*Histograms of homogenization temperatures of CO_2 of fluid inclusions from three different generations of quartz. (**A**) Pre-mineralization Q1, (**B**) Ore-stage Q2, and (**C**) Post-mineralization Q3. The data from Chi et al. (2002) are also shown.*

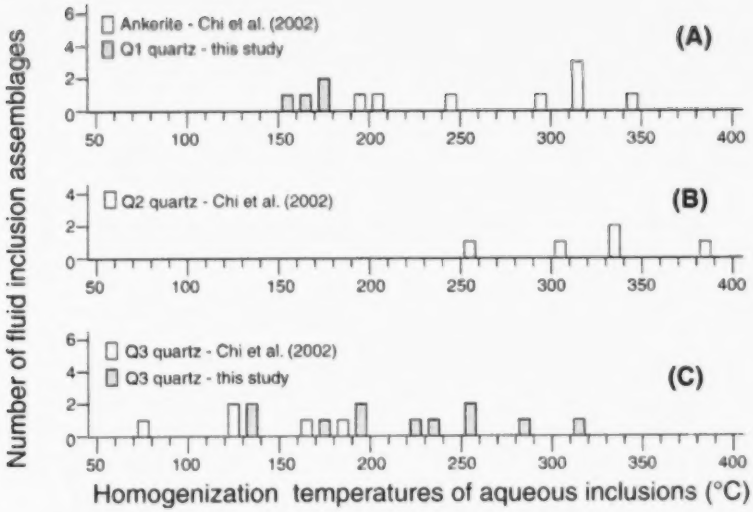
Number of fluid inclusion assemblages
Ankerite - Chi et al. (2002)
Q1 quartz - this study
(A)
Q2 quartz - Chi et al. (2002)
(B)
Q3 quartz - Chi et al. (2002)
Q3 quartz - this study
(C)
Homogenization temperatures of aqueous inclusions (°C)

Figure 7.

*Histograms of homogenization temperatures of aqueous fluid inclusions from three different generations of quartz. (**A**) Pre-mineralization Q1, (**B**) Ore-stage Q2, and (**C**) Post-mineralization Q3. The data from Chi et al. (2002) are also shown.*

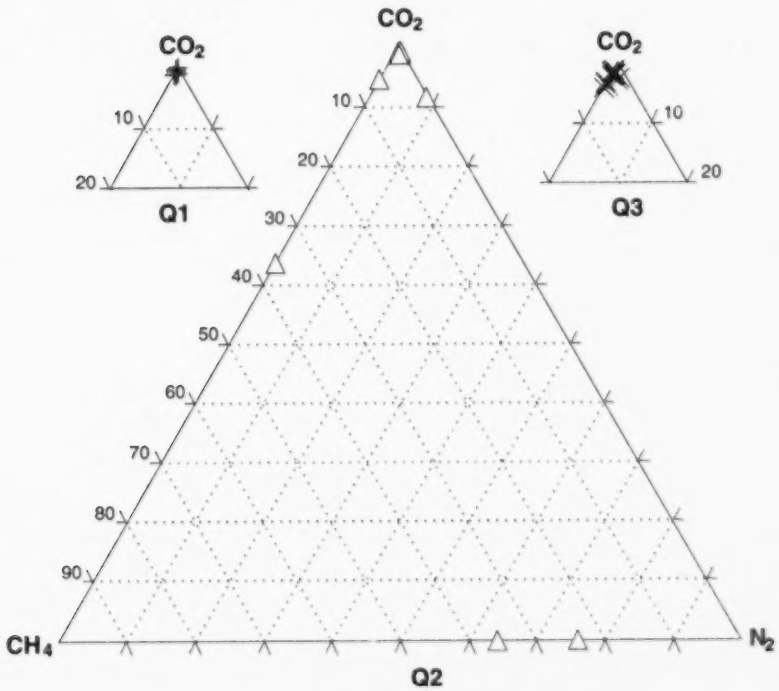

Figure 8.

The CO_2-CH_4-N_2 composition of carbonic fluid inclusions from different generations of quartz, as analysed by the laser-Raman microspectrometry.

The laser Raman analyses confirm the suggestion of the microthermometric data that the carbonic fluid inclusions are dominated by CO_2 for all the three different generations of quartz. Nevertheless, some compositional differences are observed among Q1, Q2, and Q3. Fluid inclusions in Q1 generally contain less than 1 mol % of CH_4 and no or trace amounts of N_2. Fluid inclusions in Q2 are more variable in composition. Most of them are dominated by CO_2 and contain trace amounts of CH_4 and N_2. However, some of them contain significant amounts of CH_4 and N_2, and some are even dominated by CH_4 and N_2 (Fig. 8). Fluid inclusions in Q3 are similar to some in Q2 in that they are dominated by CO_2 and contain both CH_4 and N_2. However, fluid inclusions in Q3 differ from the others by the presence of trace amounts

Table 2. Gas composition of fluid inclusions analysed with laser-Raman.

Sample no.	Inclusion no.	CO_2 (%mol)	CH_4 (%mol)	N_2 (%mol)	H_2S (%mol)	C_2H_6 (%mol)
KG00-50-5	KG00-50-5-b6	99.0	1.0	nd		
(Q1)	-b7	99.2	0.8	nd		
	-b8	99.2	0.8	nd		
	-b11	99.2	0.8	nd		
	-b13	99.3	0.7	nd		
	-b14	99.2	0.8	nd		
	-b18	99.2	0.3	0.5		
	-b24	99.0	0.9	< 0.2		
	-b25	99.5	0.5	nd		
	-b31	99.7	0.3	nd		
	average	99.3	0.7			
RP94-20A	RP94-20A-a1	100.0	nd	nd		
(Q1)	-a2	100.0	nd	nd		
	-a3	> 99.5	0.5	nd		
	average	100.0				
Average Q1		99.6	0.4			
KG00-11	KG00-11-a3	99.0	0.4	0.6		
(Q2)	-a5	99.0	0.4	0.6		
	KG00-11-b6	99.5	0.4	< 0.2		
	-b7	99.0	0.6	0.4		
	-b4	nd	24.0	76.0		
	-b5	nd	36.0	64.0		
	-b8	99.2	0.2	0.6		
	KG00-11-c1	94.5	5.5	nd		
	-c3	99.0	0.1	0.9		
	-c1'	63.5	36.5	nd		
	-c3'	91.5	0.1	8.5		
	average	76.7	9.5	13.8		
Kg00-51A	KG00-51A-b1	96.5	3.5	nd		
(Q3)	-b2	96.5	3.5	nd		
	-b4	96.8	3.2	nd		
	-b5	96.4	3.6	nd		
	-b6	96.6	3.4	nd		
	-b7	96.4	3.6	nd	≤ 0.1	≤ 0.05
	-b8	96.0	4.0	nd		≤ 0.05
	-b9	96.4	3.6	nd		≤ 0.05
	KG00-51A-c2	98.5	1.4	< 0.2	≤ 0.1	
	-c3	98.5	1.4	< 0.2	≤ 0.1	
	-c5	98.5	1.4	< 0.2	≤ 0.1	
	-c6	98.4	1.5	< 0.2	≤ 0.1	
	-c7	98.0	1.7	0.3	≤ 0.1	
	-c8	98.0	1.7	0.3	≤ 0.1	
	-c9	97.5	1.1	1.4		
	-c10	98.4	1.3	0.3		
	-c11	96.3	1.3	1.4		
	-c12'	98.5	1.5	nd	≤ 0.1	
	-c13	98.3	1.0	0.7		
	-c14	97.8	2.1	< 0.2	≤ 0.1	
	-c15	98.8	1.1	< 0.2	≤ 0.1	
	-c20	98.3	1.5	< 0.2	≤ 0.1	
	-c21	98.2	1.5	< 0.2	≤ 0.1	
	-c24	98.3	1.5	< 0.2		
	-c25	96.3	3.3	0.4	≤ 0.1	
	average	97.5	2.2	0.3		
nd : not detected						

of H_2S and/or C_2H_6 (Table 2). The presence of H_2S in aqueous inclusions is also indicated by the anomalously high melting temperatures of clathrates (Table 1).

PRESSURE REGIMES AND DISCUSSION

The isochores of carbonic inclusions, approximated by the CO_2-N_2-CH_4 system, are constructed using the gas composition (Table 2) and homogenization temperatures of the carbonic phase (Table 1), with the equation of state of Holloway (1981). For inclusions where laser Raman analysis is unavailable, their gas compositions are approximated by the average of the sample. For samples Core-A2, Core-A3, and BD20-98A, which have not been analyzed by laser Raman microspectrometry, their gas composition is approximated by CO_2. The ranges of isochores for individual samples are shown in Figure 9. We will use these isochores to discuss two problems: the depths of carbonate veining and mineralization, and the fluctuation of fluid pressures.

Depth of carbonate veining and gold mineralization

The co-existence of carbonic and aqueous fluid inclusions and the predominance of carbonic fluid inclusions have been previously interpreted as resulting from fluid-phase separation and preferential trapping of the carbonic phase (Tarnocai, 2000; Chi et al., 2002). However, the absence of visible aqueous phase in the carbonic inclusions (even in very large ones, e.g. 55 mm, *see* Table 1), in conjunction with the virtual absence of aqueous fluid inclusions, suggests that the carbonic fluids may have been unsaturated with water (Chi

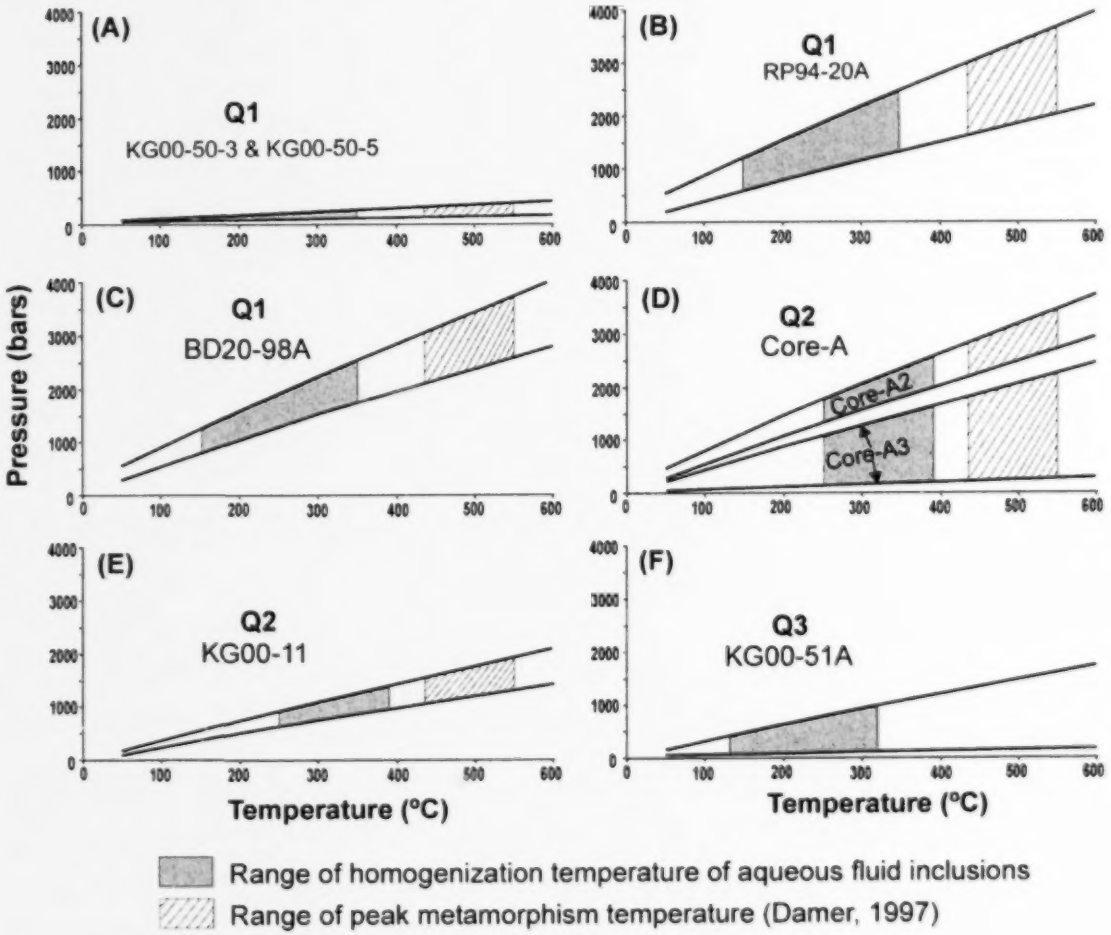

Figure 9. *Isochores of carbonic fluid inclusions from different samples and stages. Shaded areas indicate range of temperatures and pressures based on homogenization temperatures of aqueous fluid inclusions (gray area) and peak metamorphism temperatures (hatched area; 435 to 550°C: Damer, 1997).*

of H_2S and/or C_2H_6 (Table 2). The presence of H_2S in aqueous inclusions is also indicated by the anomalously high melting temperatures of clathrates (Table 1).

PRESSURE REGIMES AND DISCUSSION

The isochores of carbonic inclusions, approximated by the CO_2-N_2-CH_4 system, are constructed using the gas composition (Table 2) and homogenization temperatures of the carbonic phase (Table 1), with the equation of state of Holloway (1981). For inclusions where laser Raman analysis is unavailable, their gas compositions are approximated by the average of the sample. For samples Core-A2, Core-A3, and BD20-98A, which have not been analyzed by laser Raman microspectrometry, their gas composition is approximated by CO_2. The ranges of isochores for individual samples are shown in Figure 9. We will use these isochores to discuss two problems: the depths of carbonate veining and mineralization, and the fluctuation of fluid pressures.

Depth of carbonate veining and gold mineralization

The co-existence of carbonic and aqueous fluid inclusions and the predominance of carbonic fluid inclusions have been previously interpreted as resulting from fluid-phase separation and preferential trapping of the carbonic phase (Tarnocai, 2000; Chi et al., 2002). However, the absence of visible aqueous phase in the carbonic inclusions (even in very large ones, e.g. 55 mm, *see* Table 1), in conjunction with the virtual absence of aqueous fluid inclusions, suggests that the carbonic fluids may have been unsaturated with water (Chi

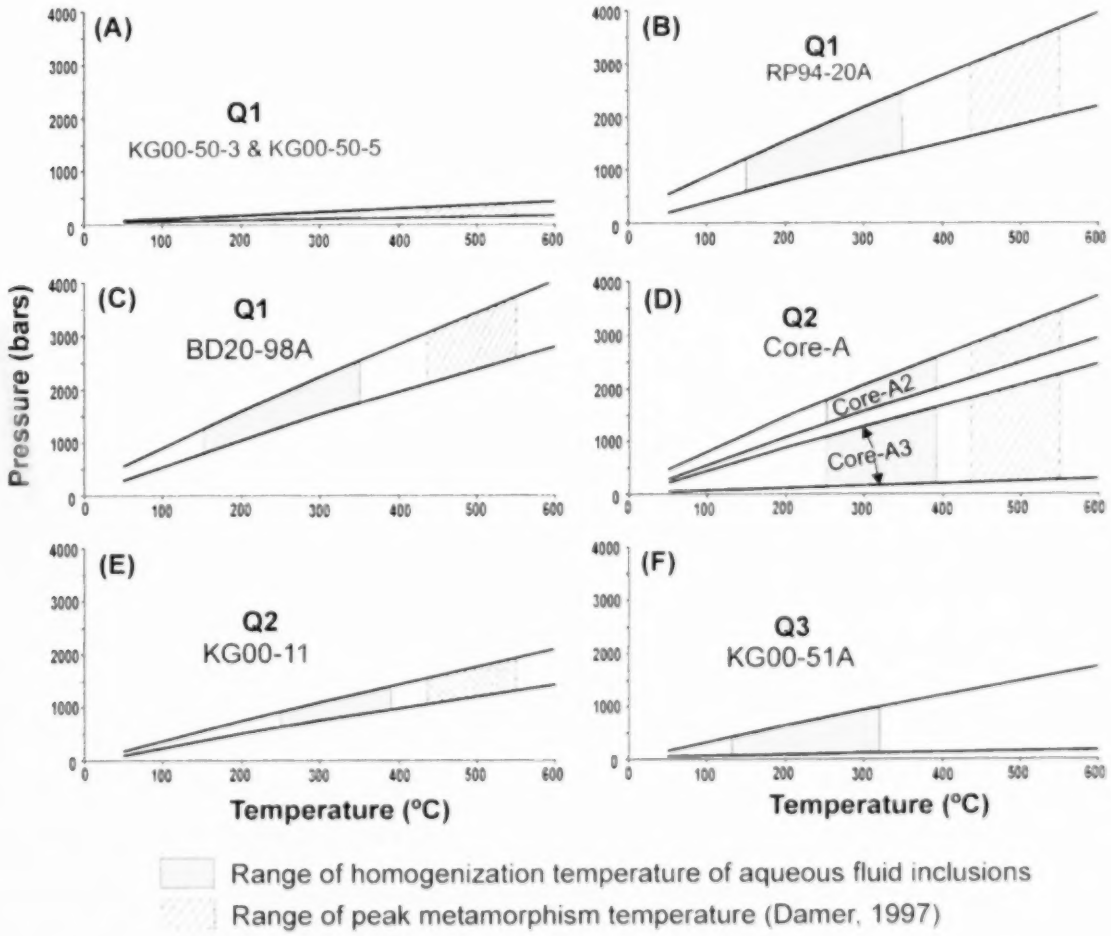

Figure 9. *Isochores of carbonic fluid inclusions from different samples and stages. Shaded areas indicate range of temperatures and pressures based on homogenization temperatures of aqueous fluid inclusions (gray area) and peak metamorphism temperatures (hatched area; 435 to 550°C; Damer, 1997).*

et al., work in progress). Similar situations have been reported in a few other gold deposits, including the giant Ashanti gold deposit (Schmidt Mumm et al., 1997), but the causes of water deficiency in the carbonic inclusions have been controversial (Klemd, 1998; Schmidt Mumm et al., 1998). If the carbonic inclusions were unsaturated with water at entrapment, then the aqueous inclusions must have been entrapped at a different time, and their homogenization temperatures represent the minimum temperatures of the fluids. Using the ranges of T_h values of the aqueous inclusions, i.e. 150° –350°C, 250° –390°C, and 131°–320°C, for Q1, Q2, and Q3 stages, respectively (Fig. 7), the pressures estimated from the isochors (Fig. 9) range from 74–2706, 155–2574, and 68–1000 bars for the three stages, respectively. The maximum pressure values (2706, 2574, and 1000 bars) correspond to a lithostatic burden (assuming a density of 2.7 g/cm^3) of 10.2, 9.7, and 3.8 km, respectively. Because the T_h values of the aqueous inclusions probably represent the minimum temperatures of the Q1 and Q2 fluids, the actual temperatures may have been higher than 350–390°C. Dubé et al. (2001, 2002, 2003) have proposed that carbonate veining is mainly a pre- to early-D_2 event, whereas high-grade gold mineralization and associated silicification are mainly syn-D_2. Sanborn-Barrie et al. (2001) have shown that the timing of D_2 is ca. 2.72 Ga, which is broadly the same as regional metamorphism. Dubé et al. (2001, 2002) have shown that several carbonate veins in the Goldcorp Inc. High Grade zone were boudinaged with amphiboles in the pull-apart, and that the high-grade gold-bearing silicification is broadly syn- to post-boudinage of the carbonate veins. These chronological relationships suggest that the high-grade gold mineralization is at least in part syn-D_2 deformation and metamorphism. The temperatures of amphibole-grade regional metamorphism have been estimated at the Red Lake mine at 435°–550°C (Damer, 1997). Using this temperature range and the isochores of carbonic fluid inclusions (Fig. 9), the maximum fluid pressures for Q1 and Q2 are up to 3.1–3.7 kbar and 2.8–3.4 kbar, respectively, corresponding to a lithostatic burden (assuming a density of 2.7 g/cm^3) of 11.7–14.0 km and 10.6–13.5 km, respectively.

The difference between homogenization temperatures of aqueous fluid inclusions (maximum 390°C) and metamorphic temperature (435°–550°C) may suggest diachroism between mineralization and peak metamorphic conditions (i.e. the mineralization could be pre-peak metamorphic or associated with post-peak metamorphism retrograde cooling), or the limited homogenization temperatures measured only represent the minimum temperature of the ore-forming fluids. However, either using the homogenization temperatures of aqueous fluid inclusions or the metamorphic temperatures, the maximum fluid pressures estimated from the isochores of carbonic fluid inclusions indicate moderate to deep environments.

The overall characteristics of fluid composition and temperature-pressure conditions estimated from the fluid inclusions are compatible with those proposed for the orogenic type gold deposits (Groves et al., 2003). The open-space filling textures (cockade and crustiform) from the Campbell-Red Lake deposit are similar to the Wiluna lode-gold deposits, which have been cited as examples of shallow-level or epizonal (<5 km) part of the spectrum of orogenic-type lode-gold deposits (Hagemann et al., 1994; Hagemann and Cassidy, 2000). However, as shown above, the isochores of carbonic fluid inclusions combined with the homogenization temperatures of limited aqueous inclusions suggest depths >5 km. A more accurate estimation of the depth is, however, hindered by the uncertainty on fluid temperature.

Cause of fluid-pressure fluctuation

As shown by the ranges of isochores of carbonic fluid inclusions (Fig. 9), there is a tremendous variation of fluid pressures in every stage of the hydrothermal activities. A primary suspect causing such variations is, as discussed in Chi et al. (2002), post-trapping stretching of the carbonic fluid inclusions, which results in lower density of the fluid in the inclusions and hence isochores with lower pressure values. Although post-trapping stretching may have affected the fluid inclusions, the authors do not think it is the cause of the fluid-pressure variation indicated in Figure 9, based on the following reasons. Firstly, in contrast to the overall large variation, T_h-CO_2 values within individual fluid inclusion assemblages are relatively consistent (Table 1). Secondly, some samples (KG00-50-3 and KG00-50-5) consistently show homogenization of the carbonic fluid into the vapour phase (Table 1), indicating low fluid pressures (Fig. 9A). This consistency argues against the fluid inclusions being all resulting from stretching of higher-density fluid inclusions (which do not exist in the same crystals). Finally, the systematic lowering of fluid pressures from quartz predating (Core-A2) to postdating (Core-A3) ankerite in the same sample (Fig. 9D, Core-A) suggests a real change in fluid pressure during the filling of the vein.

The fluid pressure fluctuation may be related to episodic change of the pressure systems between lithostatic and hydrostatic ones, as illustrated in the fault-valve model of Sibson et al. (1988). However, the maximum and minimum pressures shown in Figure 9 at any given temperatures are more than 2.7 times different, which is more than what can be accounted for by the lithostatic-hydrostatic change (lithostatic pressures are 2.7 time hydrostatic pressures) for a given temperature and depth. Although changing depths and temperatures may be partly responsible for this discrepancy, we tentatively propose that the fluid pressures may have been temporarily below hydrostatic values at times during the history of the hydrothermal activities. Such sub-hydrostatic pressure regimes may have been produced periodically in relation to sudden opening of fractures associated with local extensional stresses. The structural location of at least part of the carbonate veins and high-grade auriferous silicic replacement ore, i.e., at high-angle to the folded Balmer basalt and basaltic komatiites contacts in the hinge area of the F2 folds, may have

favours the periodic opening and sealing of extensional fractures (Dubé et al., 2001, 2002, 2003). The formation of crustiform and cockade cavity-fill textures may have been related to such local extensional strain regimes. The protracted structural activities along the Red Lake Mine Trend may have resulted in repeatedly low-pressure regimes, thus sucking and focusing the mineralizing fluids along the hydrothermal corridor and low pressure area.

Gold transportation and precipitation

Although this study focuses on fluid pressure regimes, the fluid-inclusion data raise some questions about the transportation and precipitation of gold. Firstly, the absence of visible aqueous phase in the carbonic inclusions and the extreme scarcity of aqueous fluid inclusions in the Q1 and Q2 stages suggest that the carbonic fluids may have been deficient in water (Chi et al., work in progress). The Raman analyses indicate no detectable H_2S in the carbonic fluids of Q1 and Q2 stage. The gold-transporting capacity of such water-deficient carbonic fluids is unknown, as discussed by Schmidt Mumm et al. (1997, 1998) and Klemd (1998) for the Ashanti gold deposit. On the other hand, the overall similarity between the giant Campbell-Red Lake and Ashanti deposits in terms of fluid inclusions raises the possibility that maybe the apparently water-deficient carbonic fluids are extremely good gold-carrier, noting that the Campbell-Red Lake deposit is also famous for its high-grade gold mineralization (Dubé et al., 2002). In this regard, it is worth noting that Au, Cu, As and B have the tendency of being selectively partitioned into the vapour in a boiling magmatic fluid system (Heinrich et al., 1999), suggesting that vapour-rich fluids can be very good gold carriers. Secondly, if the carbonic fluids from Q1 and Q2 were unsaturated with water at entrapment, they are unlikely to have been derived from in situ phase separation, and thus phase-separation as a mechanism of gold precipitation (e.g., Robert and Kelly, 1987) may not apply here. A two-stage model involving first a phase separation and partitioning of Au into the vapour phase (before fluids entering the site of mineralization) and then precipitation of gold from the gas-rich phase may be envisaged, which needs further examination. Thirdly, the Raman analyses indicate that the carbonic fluids from Q2 (ore-stage) are enriched in CH_4 and N_2 compared to those in Q1 (pre-ore) (Fig. 8). The enrichment of CH_4 over CO_2 has been observed in many other mesothermal-orogenic gold deposits (e.g., Guha et al., 1991). The redox reactions associated with the CH_4 enrichment may be responsible for gold precipitation. Finally, although fluid inclusions from Q3 partly overlap those from Q1 and Q2 in terms of temperature, pressure and bulk composition, there are two significant differences: 1) in addition to carbonic fluid inclusions, Q3 contains significant number of aqueous fluid inclusions, suggesting that the fluid system changed from a "dry" (water-deficient) to "wet" one; and 2) the carbonic fluid inclusions in Q3 contain detectable H_2S, which may be, at least in part, responsible for gold remobilization in the post-ore stage as HS complexes.

CONCLUSIONS

The fluid-inclusion data suggest that the pre-ore carbonate veining and high-grade ore-stage silicification probably took place at moderate to considerable depths >5 km and is compatible with orogenic gold deposits (Groves et al., 2003). A more accurate estimation of the depth is, however, hindered by the uncertainty on fluid temperature. Extremely large variations of fluid pressures probably reflect alternating lithostatic and sub-hydrostatic pressure regimes, which is related to the protracted structural and hydrothermal activities within the Campbell-Red Lake deposit of the Red Lake Mine Trend. The apparent absence of aqueous phase in carbonic fluid inclusions and the extreme scarcity of aqueous inclusions in the pre-ore and ore-stage minerals have raised some questions about the transportation and deposition of gold in 'dry' (water-deficient) and extremely rich carbonic fluids with CH_4 and N_2, which need to be further examined.

ACKNOWLEDGEMENTS

We would like to thank the staff of Goldcorp Inc., in particular Gilles Filion, Stephen McGibbon, Rob Penczak, Tim Twomey, John Kovala, Mark Epp, Michael Dehn, Matt Ball, for their scientific contribution, logistic and financial support and permission to publish. Rob Penczak is especially thanked for sharing his knowledge of the entire Campbell-Red Lake deposit and for providing some of the samples included in this study. Michel Malo, Mary Sanborn-Barrie, Tom Skulski, Jack Parker, François Robert, Howard Poulsen, Jean-François Couture, Vic Wall and Nick Archibald are thanked for constructive discussions. Critical review by Jayanta Guha improved the manuscript.

REFERENCES

Andrews, A.J., Hugon, H., Durocher, M., Corfu, F., and Lavigne, M.
1986: The anatomy of a gold-bearing greenstone belt: Red Lake, northwestern Ontario; *in* Proceedings of Gold '86, an International Symposium on the Geology of Gold Deposits, Konsult International, Inc, Toronto, Canada, p. 3–22.

Bény, C., Guilhaumou, N., and Touray, J.-C.
1982: Native-sulphur-bearing fluid inclusions in the CO_2-H_2S-H_2O-S system — microthermometry and Raman microprobe (MOLE) analysis — thermochemical interpretations; Chemical Geology, v. 37, p. 113–127.

Chi, G., Dubé, B., and Williamson, K.
2002: Preliminary fluid-inclusion microthermometry study of fluid evolution and temperature-pressure conditions in the Goldcorp High-Grade zone, Red Lake mine, Ontario; Geological Survey of Canada, Current Research, 2002-C27, 12 p.

Damer, G.C.
1997: Metamorphism of hydrothermal alteration at the Red Lake Mine, Balmertown, Ontario; M.Sc. thesis, Queen's University, Kingston, Ontario, 195 p.

Dubé, B., Williamson, K., and Malo, M.
2001: Preliminary report on the geology and controlling parameters of the Goldcorp Inc. High Grade zone, Red Lake mine, Ontario; Geological Survey of Canada, Current Research, 2001-C18, 23 p.
2002: Geology of the Goldcorp Inc. High-Grade zone, Red Lake mine, Ontario: an update; Geological Survey of Canada, Current Research, 2002-C26, 13 p.

Dubé, B., Williamson, K., and Malo, M. (cont.)
2003: Gold mineralization within the Red Lake mine trend: example from the Cochenour–Willans mine area, Red Lake, Ontario, with new key information from the Red Lake mine and potential analogy with the Timmins camp; Geological Survey of Canada, Current Research, 2003-C21, 15 p.

Goldstein R.H. and Reynolds T.J.
1994: Systematics of fluid inclusions in diagenetic minerals; Society for Sedimentary Geology (SEPM) Short Course Notes, 31, p. 1–199.

Groves, D.I., Goldfarb, R.J., Robert, F., and Hart, G.J.R.
2003: Gold deposits in metamorphic belts: overview of current understanding, outstanding problems, future research, and explorations significance; Economic Geology, v. 98, p. 1–29.

Guha, J., Lu, H.-Z., Dubé, B., Robert, F., and Gagnon, M.
1991: Fluid characteristics of vein and altered wall rock in Archean Mesothermal gold deposits; Economic Geology, v. 86, p. 667–684.

Hagemann, S.G. and Cassidy, K.F.
2000: Archean orogenic lode gold deposits, *in* Gold in 2000, (ed.) S.G. Hagemann and P.E. Brown; Review *in* Economic Geology, v. 13, p. 9–68.

Hagemann, S.G., Gebre-Mariam, M., and Groves, D.I.
1994: Surface-water influx in shallow-level Archean lode-gold deposits in Western Australia; Geology, v. 22, p. 1067–1070.

Heinrich, C.A., Günther, D., Audédat, A., Ulrich, T., and Frischknecht, R.
1999: Metal fractionation between magmatic brine and vapour, determined by microanalysis of fluid inclusions; Geology, v. 27, p. 755–758.

Holloway J.R.
1981: Compositions and volumes of supercritical fluids in the earth's crust; *in* Fluid Inclusions: Applications to Petrology, (ed.) L.S. Hollister & M.L. Crawford, Mineralogical Association of Canada, Short Course Handbook 6, p. 13–38.

Klemd, R.
1998: Comment on the paper by Schmidt Mumm et al. 'High CO_2 content of fluid inclusions in gold mineralisations in the Ashanti Belt, Ghana: a new category of ore forming fluids? (Mineralium Deposita, v. 32, p. 107–118, 1997)'; Mineralium Deposita, v. 33, p. 317–319.

MacGeehan, P. and Hodgson, C.J.
1982: Environments of gold mineralization in the Campbell–Red Lake and Dickenson mines, Red Lake district, Ontario; *in* Geology of Canadian Gold Deposits, Canadian Institute of Mining and Metallurgy, Special Volume 24, p. 184–207.

Penczak, R. and Mason, R.
1997: Metamorphosed Archean epithermal Au-As-Sb-Zn-(Hg) vein mineralization at the Campbell Mine, Northwestern Ontario; Economic Geology, v. 92, p. 696–719.

Robert, F., and Kelly, W.C.
1987: *Ore-forming fluids in Archean gold-bearing quartz veins at Sigma* mine, Abitibi greenstone belt, Quebec, Canada; Economic Geology, v. 82, p. 1464–1482.

Rogers, J.
1992: The Arthur W White Mine, Red Lake area, Ontario: detailed structural interpretation the key to successful grade control and exploration; CIM Bulletin, v. 85, no. 957, p. 37–44.

Sanborn-Barrie, M., Skulski, T., and Parker, J.
2001: Three hundred millions of years of tectonic history recorded by the Red Lake greenstone belt, Ontario; Geological Survey of Canada, Current Research 2001-C19, 19 p.

Schmidt Mumm, A., Oberthür, T., Vetter, U., and Blenkinsop, T.G.
1997: High CO_2 content of fluid inclusions in gold mineralisations in the Ashanti Belt, Ghana: a new category of ore forming fluids?; Mineralium Deposita, v. 32, p. 107–118.
1998: High CO_2 content of fluid inclusions in gold mineralisations in the Ashanti Belt, Ghana: a new category of ore forming fluids? – a reply; Mineralium Deposita, v. 33, p. 320–322.

Sibson, R.H., Robert, F., and Poulsen, K.H.
1988: High-angle reverse faults, fluid-pressure cycling, and mesothermal gold-quartz deposits; Geology, v. 16, p. 551–555.

Tarnocai, C.
2000: Archean gold mineralization at the Campbell mine, eastern Red Lake greenstone belt, western Superior Province of Canada; Ph.D. thesis, University of Ottawa, Ottawa, Ontario, 227 p.

Tarnocai, C., Hattori, K., and Stubens, T.C.
1998: Metamorphosed Archean epithermal Au-As-Sb-Zn-(Hg) vein mineralization at the Campbell Mine, northwestern Ontario - a discussion; Economic Geology, v. 96, p. 683–688.

Twomey, T. and McGibbon, S.
2002: The geological setting and estimation of gold grade of the high-grade zone, Red Lake Mine, Goldcorp Inc; Exploration and Mining Geology, v. 10, no.1-2, p. 19–34.

Zhang, G., Hattori, K., and Cruden, A.
1997: Structural evolution of auriferous deformation zones at the Campbell Mine, Red Lake greenstone belt, Superior province; Precambrian Research, v. 84, p. 83–103.

Geological Survey of Canada Project GK4500